Analytical QoT Model for Bi-Di Single-Fiber Point-to-Multipoint DSCM Coherent Systems

Esteban Paz[1,2,*], Giuseppe Parisi[1], Pablo Torres-Ferrera[1], Tiago Silvério[1,2], Sasipim Srivallapanondh[1], Miquel Masanas[1], Luis Velasco[2], M. Sezer Erkilinç[3], Roberto Magri[4] and Antonio Napoli[1]

[1]*Nokia, Germany;* [2]*Universitat Politècnica de Catalunya, Spain;* [3]*Nokia, UK;* [4]*Ericsson, Italy*

[*]*esteban.paz@nokia.com*

Abstract: We experimentally validate a transmission model for single-fiber/laser bidirectional links in next-generation mobile transport with point-to-multipoint coherent transceivers. The model achieves 0.3dB accuracy in 90% of cases, enabling reliable performance prediction and network optimization.

1. Introduction

Next-generation 6G mobile transport networks will require (i) higher throughput, (ii) lower upstream/downstream latency, and (iii) reduced hardware complexity and cost. Coherent bidirectional (Bi-Di) transmission over a single fiber and single laser is a promising solution, as it enables efficient use of scarce fiber resources while maintaining compatibility with PON architectures. Sharing the same optical medium also minimizes latency and alleviates timing and synchronization challenges envisioned for 6G [1, 2]. One of the key challenges in single laser Bi-Di is dealing with reflections – both discrete (e.g., connector induced) and distributed (Rayleigh backscattering, RBS) – with recent works proposing signaling schemes that are inherently more tolerant to reflections [3, 4]. Coherent transceivers based on Digital Subcarrier Multiplexing (DSCM) architectures offer high flexibility at the transmitter [5], supporting mixed configurations and scalable Point-to-Multipoint (P2MP) operation [6]. Coherent transceivers can deliver the required capacity, while single-laser/wavelength operation enables filterless, spectrally efficient single-fiber designs that reduce cost and complexity. Reflection-induced penalties and time-varying field conditions (e.g., contaminated connectors) make spectral flexibility essential. DSCM enables this through N Digital Subcarriers (DSCs) operating as quasi-independent channels, allowing fine-grained adaptation to instantaneous link conditions.

In this contribution, we present and experimentally validate an analytical model that supports real-time Quality of Transmission (QoT) estimation in a P2MP network with one HUB and 2 LEAFs, i.e. the central office and user segments, respectively, in single-fiber sigle-laser Bi-Di coherent optical transmission. This analytical model enables reliable performance prediction and network optimization with high accuracy.

2. Experimental setup

Fig. 1 shows the experimental setup: a Bi-Di P2MP optical network with a central HUB and two LEAF nodes (L1 and L2), over a single-fiber. The nodes employ real-time coherent DSCM with a single-laser Bi-Di architecture at 194 THz. Each transceiver (TRX) uses Dual Polarization (DP)-16QAM at 25 Gbps per DSC. The 400G HUB operates 16 DSCs; four per LEAF (100G each), while the remaining eight remain active to ensure full-capacity operation. Each LEAF uses four DSCs per direction.

A 3–dB splitter distributes traffic among nodes, and optical circulators route the transmitted and received signals to their corresponding ends. The TRXs operate at fixed output power, and three external Variable Optical Attenuators (VOAs) control the transmitted power of each node: A_H at the HUB TX, and A_{L1} and A_{L2} at the LEAFs TXs. The HUB–LEAF distances are $d_1 = 20$ km and $d_2 = 40$ km, conformed by two 20 km Standard Single Mode Fiber (SSMF) segments. System losses, A_{loss}, include fiber attenuation, splitter, and insertion losses. This setup provides

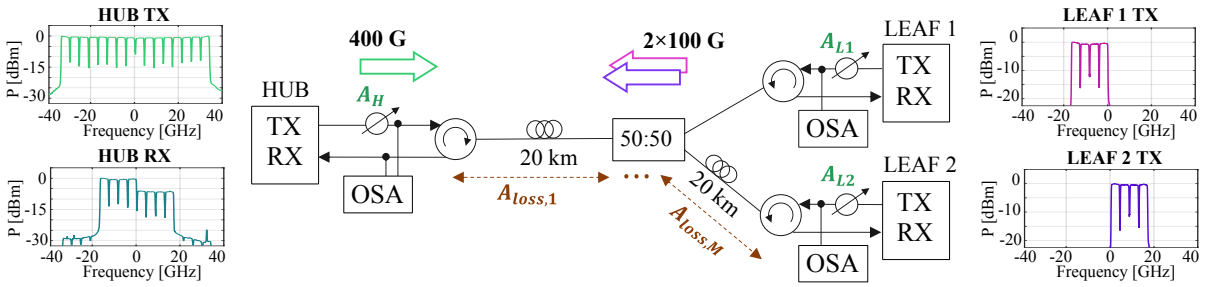

Fig. 1: P2MP setup with HUB and LEAFs showing their TX spectrum, and the RX one at the HUB.

the experimental data for validating the analytical Generalized Signal-to-Noise-Ratio (GSNR) model as function of nodes' power. Measured spectra in Fig. 1, with frequency axis relative to 194 THz, show the transmitted signals from HUB, LEAF 1, LEAF 2, and the received signal at the HUB, revealing the HUB reflections and the power imbalance between LEAFs due to different path losses (assuming same transmitted power in the LEAFs).

3. Analytical model

We derive a Bi-Di transmission model based on the Additive White Gaussian Noise (AWGN) approach [6, 7], where all interference and impairments are treated as noise. This results in $\mathrm{GSNR}^{-1} = \mathrm{SNR_{TRX}}^{-1} + \mathrm{SNR_{RBS}}^{-1} + \mathrm{SNR_{XT}}^{-1}$, with contributions from TRX intrinsic noise, RBS, and crosstalk (XT). Eq. (1) extends this model to each individual ith-DSC, considering each node's transmit–receive pair, with $P_{\mathrm{TX},i}$ and $P_{\mathrm{RX},i}$ representing the local transmit and remote receive powers along the corresponding light path.

$$\mathrm{GSNR_{DSC,i}} = \frac{P_{\mathrm{RX,i}}}{\underbrace{\alpha_{\mathrm{TRX}} + \beta P_{\mathrm{RX,i}}}_{N_{\mathrm{TRX}}} + \underbrace{\sum_{m=1}^{M} \left(2A_{\mathrm{loss},m} S \alpha_R (1 - e^{-4\alpha_m d_m})/4\alpha_m\right) P_{\mathrm{TX,i}}}_{N_{\mathrm{RB}}} + N_{\mathrm{XT}}} \tag{1}$$

The TRXs intrinsic noise is represented as a baseline noise composed of a power-independent and power-dependent term, modeled as: $\mathrm{N_{TRX}} = \alpha_{\mathrm{TRX}} + \beta \mathrm{P_{RX}}$ [8]. Parameters α_{TRX} and β are fitted from the experimental GSNR and $\mathrm{P_{RX}}$ data points for each individual transmitter-receiver pair, measured while isolating other interference sources (RBS and crosstalk).

RBS is a key interference source in Bi-Di networks and can be modeled as AWGN. This assumption holds in coherent systems, where backscattered light is depolarized, approximately spectrally flat over the signal band, and uncorrelated with the signal of interest [9]. Localized fiber discontinuities such as splices or connectors may introduce discrete reflections that further degrade signal quality [6]. Here, we neglect the impact of discrete reflections as they cannot be predicted, but in practical systems a proper SNR margin should be reserved to account for such reflections. The equivalent reflectivity of the distributed RBS is defined as $N_{RB} = P_{\mathrm{TX,i}} \cdot 2A_{loss} S \alpha_R (1 - e^{-4\alpha d})/(4\alpha)$, where α is the fiber attenuation coefficient, $S = 1.5 \cdot 10^{-3}$ and $\alpha_R \approx 0.15[\mathrm{dB/km}]$ are the RB capture factor and RB field loss, respectively. This estimate applies to a single fiber segment, and for a system with M segments, $N_{RB,m}$ must be computed individually using each segment's loss $A_{\mathrm{loss},m}$, and then all contributions summed. Total system losses include fiber attenuation, splitters, and insertion losses, but here $A_{\mathrm{loss},m}$ refers only to component losses within the segment, as fiber attenuation α_m is already included in the exponential term.

The XT term, N_{XT}, between the channels is attributed to out-of-band noise generated at the TX of each channel. Although colored, this term is approximated as locally AWGN and it is estimated by direct experimental measurement, e.g., during qualification testing.

4. Experimental results against analytical model

We experimentally measured the Q-factor for all DSCs in the network. The minimum Q-factor among them is adopted as the system performance metric, as it defines the overall transmission limit by representing the lowest-performing DSC, as expressed in (2).

$$\mathrm{Q^2_{min}}(\mathrm{A_{L1}}, \mathrm{A_{L2}}, \mathrm{A_H}) = \min\left\{\mathrm{Q^2_{L1\to H}}, \mathrm{Q^2_{L2\to H}}, \mathrm{Q^2_{H\to L1}}, \mathrm{Q^2_{H\to L2}}\right\}, \tag{2}$$

The experimental values are obtained from TRX measurements, while the analytical ones are derived from the modeled GSNR from Eq. (1) as $\mathrm{Q} = \sqrt{2} \cdot \mathrm{erfc}^{-1}[3/4 \cdot \mathrm{erfc}(\sqrt{\mathrm{GSNR}/10})]$, corresponding to DP-16QAM modulation. Each term $\mathrm{Q^2_{A\to B}}$ contains the Q-factor of the DSCs received at node B from node A.

Fig. 2 shows the experimentally measured $\mathrm{Q^2_{min}}$ (solid lines) and analytical results from the model (dashed lines) as a function of the attenuations $\mathrm{A_{L1}}$ and $\mathrm{A_{L2}}$ for six $\mathrm{A_H}$ values. The DSC performance of HUB and LEAF nodes evolves differently with transmitted power due to the combined effects in Eq. (1). For instance, raising the transmitted power increases the SNR at one node, but simultaneously amplifies reflections and crosstalk at others, leading to a complex trade-off, where an optimal operating point can be identified such that $\mathrm{Q^2_{min}}$ is maximized for specific attenuation settings, defined as $(\mathrm{A_{L1,opt}}, \mathrm{A_{L2,opt}}) = \arg\max_{\mathrm{A_{L1}}, \mathrm{A_{L2}}} \{\mathrm{Q^2_{min}}(\mathrm{A_{L1}}, \mathrm{A_{L2}}, \mathrm{A_H})\}$.

The plots reveal that the optimal operating point shifts diagonally with increasing transmitted power, requiring a proportional LEAF-power adjustment– offset by LEAFs 2 longer path– to balance performance, while compensating for stronger reflections. Beyond a certain HUB power, the maximum $\mathrm{Q^2_{min}}$ saturates, limited by TRX noise, since for $P_{\mathrm{RX}} \to \infty$, $\mathrm{GSNR} \to 1/\beta$ in (1), neglecting nonlinearities. At low HUB powers, e.g., $\mathrm{A_H}$ = 4–5 dB, $\mathrm{Q^2_{min}}$ is limited by low received power. These trends are further discussed in [4], and properly captured by our model.

To validate the model, we compare analytical and experimental data using Q-factor measurements within the minimum threshold. The close overlap between dashed (model) and solid (experimental) contour lines indicates

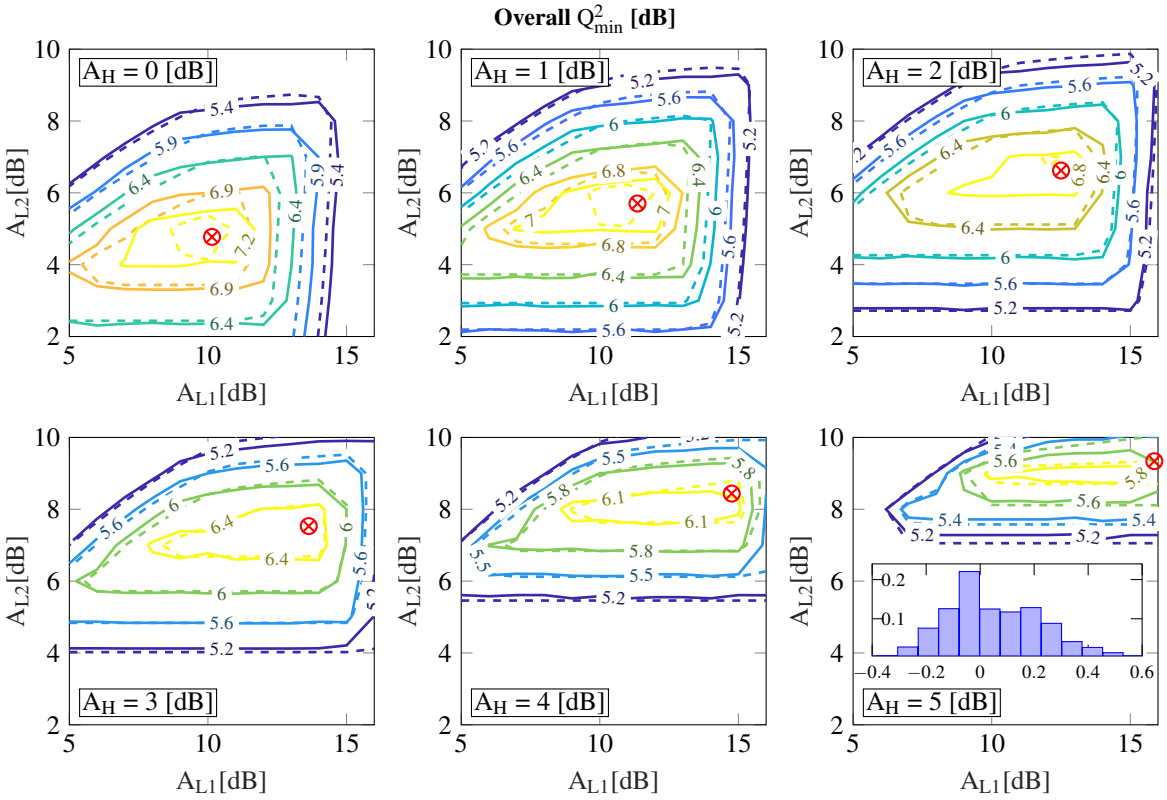

Fig. 2: Overall Q^2_{min} for all DSCs versus L1 and L2 attenuation (axes) for different Hub settings (subplots). Solid and dashed lines: experimental and modeled values. Inset: histogram of cumulative model error.

that the model accurately reproduces the measured results. The inset in the last subplot shows the model error, $E = Q_{model}[dB] - Q_{data}[dB]$, including all measured and modeled Q values (i.e. not just the Q^2_{min} ones). The histogram reveals that 90% of the errors fall within ± 0.3 dB, with all confined between -0.4 and 0.6 dB, indicating that larger deviations are very rare and the model is statistically reliable.

Finally, we employ an optimization approach following the Nelder–Mead Simplex Method [10], using the modeled GSNRs to directly find the TX power settings that maximizes the Q^2_{min}. The resulting points are shown in red markers in Fig. 2. This approach is significantly faster than the grid search approach, and can significantly simplify optimization in larger networks with multiple HUBs and LEAFs. Beyond power optimization for maximizing the Q^2_{min}, the model also enables practical strategies to optimize the DSCM management—e.g., minimizing reflections, maximizing capacity on demand, or reducing power consumption by disabling unused DSCs—which remains an open topic for future work.

5. Conclusions

We presented a BiDi P2MP analytical model capturing TRX noise, RBS, and crosstalk, validated against experimental data. For 90% of cases, the modeling error remains within ± 0.3dB. Moreover, it enables direct optimization of power settings for fast, reliable network operation and high transmission quality, even in larger networks, supporting scalable beyond-5G/6G deployments.

Acknowledgments The authors acknowledge the support of the EU Horizon Europe research and innovation programs, ALLEGRO project (GA No.101092766), MSCA-DN NESTOR (GA No.101119983). We also acknowledge the BMBF INTENSE project (GA 16KIS2221K).

References

1. F. Cavaliere *et al.* (2024) MOPA, Technical paper on Coherent lite for mobile networks.
2. T. Duthel *et al.*, "DSP design for coherent optical point-to-multipoint transmission," *JLT*, vol. 42, no. 3, 2024.
3. M. Masanas *et al.*, "Rayleigh backscattering rejection in single-laser homodyne transceiver for..." *IEEE PTL*, 2021.
4. P. Torres-Ferrera *et al.*, "Single-fiber single-wavelength bidirectional digital subcarrier point..." in *ECOC*, 2025.
5. D. Welch *et al.*, "Digital subcarrier multiplexing: Enabling software-configurable optical..." *JLT*, vol. 41, no. 4, 2023.
6. P. Torres-Ferrera *et al.*, "Impact and mitigation of reflections in 400G single-fiber bidirectional..." in *ECOC 2024*, 2024.
7. A. Carena *et al.*, "Modeling of the impact of nonlinear propagation effects..." *JLT*, vol. 30, no. 10, pp. 1524–1539, 2012.
8. L. Galdino *et al.*, "On the limits of digital back-propagation in the presence of..." *Optics Express*, vol. 25, no. 4, 2017.
9. E. Virgillito *et al.*, "Propagation impairment in single-wavelength, single-fiber bidirectional..." in *Optica APC*, 2022.
10. J. C. Lagarias *et al.*, "Convergence properties of the nelder-mead..." *SIAM Journal on Optimization*, vol. 9, no. 1, 1998.